Applied Catalysis B: Environmental 163 (2015) 96–104

Contents lists available at ScienceDirect

Applied Catalysis B: Environmental

journal homepage: www.elsevier.com/locate/apcatb

Pristine carbon nanotubes as non-metal electrocatalysts for oxygen evolution reaction of water splitting

Yi Cheng[a], Changwei Xu[a], Lichao Jia[a], Julian D. Gale[b,*], Lili Zhang[c], Chang Liu[c], Pei Kang Shen[d], San Ping Jiang[a]

[a] Fuels and Energy Technology Institute & Department of Chemical Engineering, Curtin University, Perth, WA 6102, Australia
[b] Nanochemistry Research Institute, Department of Chemistry, Curtin University, PO Box U1987, Perth, WA 6845, Australia
[c] Institute of Metal Research, Chinese Academy of Sciences, Shenyang 110016, China
[d] Advanced Energy Materials Laboratory, Sun Yat-sen University, Guangzhou 510275, China

ARTICLE INFO

Article history:
Received 22 April 2014
Received in revised form 26 June 2014
Accepted 24 July 2014
Available online 1 August 2014

Keywords:
Water electrolysis
Carbon nanotubes
Oxygen evolution reaction
Volcano curve
Electron tunneling effect

ABSTRACT

Oxygen evolution reaction (OER) is one of the most important reactions in electrochemical energy storage and conversion systems. Thus, the development of efficient electrocatalysts with high activity and durability is of great technological and scientific significance. We demonstrate here for the first time that pristine carbon nanotubes (CNTs) composed of between 2 and 7 concentric tubes and an outer diameter of 2–5 nm have an outstanding activity for the OER in alkaline solution as compared with single-walled and multi-walled CNTs (SWNTs & MWNTs). For example, current density measured at 1.8 V (vs RHE) for the OER on triple-walled CNTs is 56 mA cm^{-2}, ~10 times higher than 5.9 mA cm^{-2} measured on SWNTs and 35 times higher than 1.6 mA cm^{-2} measured on MWNTs. The activity of such CNTs is significantly higher than that of conventional 20% Ru/C and 50% Pt/C electrocatalysts at high polarization potentials. Such CNTs also show an excellent stability toward OER. One hypothesis is that for the OER on CNTs with specific number of walls, efficient electron transfer occurs on the inner tubes of the CNTs most likely through electron tunneling between outer wall and inner tubes, significantly promoting the charge transfer reaction of OER at the surface of outer wall of the CNTs. For SWNTs, such separation of functionality for OER is not possible, while effective electron tunneling between outer wall and inner tubes of the CNTs diminishes as the number of walls increases due to the reduced dc bias (i.e., the driving force) across the walls or layers of MWNTs. This hypothesis is strongly supported by the observed distinctive volcano-type dependence of the electrocatalytic activity and turnover frequencies (TOF) of CNTs as a function of number of walls.

1. Introduction

Hydrogen production from water splitting driven by renewable energy, such as hydro, solar or wind power is a most environmental friendly pathway to meet the constantly growing demand for renewable energy storage and conversion technologies. For example, the most mature solar-driven water splitting technology is the combination of commercial photovoltaic (PV) modules with water electrolyzers [1]. However, the practical application of water electrolysis or water splitting is greatly constrained by the high overpotentials (η) required and the slow rate of the oxygen evolution reaction (OER) because the release of O_2 involves the formation of an oxygen–oxygen bond with an overall four-electron process [2]. Hence, developing efficient catalysts with high activity and durability for OER is of great technological and scientific significance in the application of renewable energy storage and conversion technologies.

There are substantial progresses on developing electrocatalysts for water splitting through decades of sustained efforts. This includes noble metals and metal oxides-based OER catalysts, such as Pt [3,4], Pd [5], Au [5], Ir [4], Ru [4], RuO_2 [6], IrO_2 [7] and their combination [8], but their wide spread application is limited due to their high cost and scare resources. Water splitting under alkaline conditions allows the use of non-noble metals and inexpensive various oxide catalysts. Transition metal oxides, such as MnO_2 [9,10], Co_2O_3 [11,12], $NiCoO_3$ [13], Ni–Fe oxide [14] and $Fe_xCo_yNi_zO_x$ [15] have shown relatively good activity that are comparable to RuO_2 and IrO_2 in alkaline solutions. However, the low conductivity of these oxides is problematic in practical applications.

* Corresponding author. Tel.: +61 892669804; fax: +61 8 9266 1138.
E-mail addresses: j.gale@curtin.edu.au (J.D. Gale), s.jiang@curtin.edu.au (S.P. Jiang).

http://dx.doi.org/10.1016/j.apcatb.2014.07.049
0926-3373/

Carbon nanotubes (CNTs) are seamless cylinders composed of one or more curved layers of graphene with either open or closed ends. These materials have been extensively studied as catalyst supports due to their unique properties, such as large specific surface area, excellent mechanical and electrical properties [12,16–19]. Co_2O_3 particles supported on oxidized multi-walled carbon nanotubes (MWNTs) yielded a current density of 10 mA cm^{-2} at an overpotential (η) of 0.39 V in 0.1 M KOH solution [20], significantly better than Co_2O_3 nanocrystals. Ultrathin nickel–iron layered double hydroxide nanoplates supported on oxidized MWNTs achieved a current density of 10 A g^{-1} at η = 0.228 V in 1 M KOH with catalysts loading of 0.25 mg cm^{-2} [18]. Li et al. [21] developed a mononuclear ruthenium complex supported on MWNTs, which show high electrocatalystic activity and low η for water oxidation reaction. Modifying CNTs by nitrogen doping can also substantially enhance the electrocatalytic activity for the O_2 reduction reaction and OER in alkaline solutions [22,23]. However, it is generally believed that pristine CNTs without nitrogen doping or supported metal or metal oxide nanoparticles would have little electrocatalytic activity for the water oxidation reactions.

Here we demonstrate, for the first time, that the as-received pristine CNTs with a diameter of 2–5 nm and composed mainly of 2–7 concentric tubes have extremely high electrochemical activities for the OER in alkaline solutions, as compared with SWNTs and MWNTs. The results indicate that CNTs with such specific characteristics are efficient OER catalysts for water splitting in alkaline solutions.

2. Experimental

2.1. Materials

CNTs with different number of walls and diameters were obtained from commercial sources including Nanostructured & Amorphous Materials, Inc., USA, Beijing Dk Nano Technology Co., LTD, China and Shenzhen Nano, China. In order to reduce the possible effect of the metal catalysts, such as cobalt and nickel, in the CNTs samples on the OER, the as-received CNTs samples were purified as follow: 50 mg CNTs were dispersed in 50 mL HCl (30 wt%) solution before ultrasonicated for 1 h, then the dispersion was separated and the sludge was dispersed in a fresh 50 mL HCl (30 wt%) solution, followed by stirring overnight. The CNTs solids were collected and transfer into a Teflon digestion tank and 10 mL HCl solution was added and digested at 120 °C overnight. After the digestion, the CNTs were washed by fresh HCl, and then by HNO_3 for 3 times before rinsed thoroughly by DI water. The purified CNTs were dried and collected. Activated carbon (Sigma–Aldrich), graphite (Sigma–Aldrich), 50% Pt/C (Alfa Aesar), Ru/C (20 wt% Ru on Vulcan carbon black, Premetek Co.), KOH (Sigma–Aldrich), Nafion solution (5% in isopropanal and water, Sigma–Aldrich) were received and used without further treatment.

2.2. Characterization

The BET surface area of CNTs, activated carbon and graphite were characterized using a Gemini 2360 surface area analyzer. The Raman spectra were recorded in air at room temperature using a Perkin-Elmer GX FT-IR/Raman spectrometer with a back-scattered configuration and equipped with a Nd:YAG laser at 1064 nm as its light source for Raman. CNTs were characterized using a transmission electron microscope (TEM JEOL3000) operating at 200 kV. The average outer diameter (OD) and number of walls of CNTs were estimated by measuring 100 randomly chosen CNTs in the TEM images.

Thermogravimetric (TG, Q5000) analyses were performed under air upon equilibration at 100 °C for 15 min, followed by a ramp of 10 °C min^{-1} up to 800 °C to estimate the content of the impurities in the CNTs samples. The elements of the impurities or trace metals were analyzed using Inductively Coupled Plasma (ICP-OES, IRIS Intrepid II XSP, USA). The solutions for ICP analysis were prepared as follow: as-received CNTs and the purified CNTs were digested using microwave dissolver (SINEO, HDS-8G) with acid mixture containing 10 mL HNO_3 (65%), 1 mL $HClO_4$ and 2 mL HF (the procedure was set as: 150 °C, 5 min; 180 °C, 5 min; 200 °C, 10 min; and 230 °C, 20 min).

The electrochemical measurements were conducted in a three-electrode cell with a Luggin capillary, using a Gamery Reference 3000 Potentiostat. The tip of the Luggin capillary was placed 3 mm beneath the working electrode. The working electrode is prepared as follows. Generally, 1 mg of electrocatalyst was ultrasonically mixed in 2 mL Nafion solution to form a homogeneous ink, followed by pipetting 5 μL of the catalyst ink onto the surface of a glassy carbon electrode (GCE). The diameter of GCE was 5 mm. The iR drop between the working electrode and the tip of the Luggin capillary was estimated by measuring the impedance value at the frequency of 30 kHz. A Pt mesh and saturated calomel electrode (SCE) were used as the counter and reference electrodes, respectively. Potentials in the present study were given versus RHE reference electrode ($E_{RHE} = E_{vs\ SCE} + E_{SCE} + 0.059 \times pH$, where E_{SCE} = 0.247 V vs RHE at 20 °C).

The linear scan voltammetry was conducted at a sweep rate of 1 mV s^{-1} in the potential range between 0 and 1 V (vs SCE). Tafel plots were recorded at a scan rate of 1 mV s^{-1}. Before the potential scan, the electrode was initially conditioned at a potential of 0.65 V (vs SCE) for 5 min and Tafel plots were iR corrected. Impedance curves were recorded under open circuit and different dc bias with frequency range from 0.1 Hz to 100 kHz and the signal amplitude of 10 mV using a Gamery Reference 3000 Potentiostat. Electrode polarization resistance, R_P, was measured by the differences between the high and low frequency intercepts. Without specification, the catalyst loading was 0.025 mg cm^{-2} and the measurements were conducted at GCE with rotating speed of 2000 rpm. The reason for the use of low CNTs loading for the activity study is to avoid the mass transportation effect on the activity of CNTs. As shown in Fig. S1 (Supporting information), the activity of CNTs for OER increases linearly with the CNTs loading in the catalyst loading range of the present study. The chronopotentiometry were conducted at different current densities with catalysts loading of 0.1 mg cm^{-2}. For the purpose of comparison, commercial 20% Ru/C and 50% Pt/C electrocatalysts were also investigated for OER under identical conditions. The reproducibility of the electrochemical activity of the CNTs for the OER in alkaline solutions was confirmed by repeating the experiments for at least 3–5 times.

3. Results and discussion

3.1. Characterization of CNTs

Fig. 1 is the TEM micrographs of CNTs samples used in the present study. According to the TEM images, no metal nanoparticles were observed, indicating the good purity of the CNTs samples. The outer diameter, OD and number of walls were taken as the average of the measurement from the TEM images (Figs. S2 and S3, Supporting information). Based on the size distribution, the CNTs were categorized as belonging to one of several different groups labeled as CNTs-*n*, where *n* = 1–7. CNTs-1 mainly consists of single-walled CNTs (SWNTs, 79%), some double-walled CNTs (DWNTs, 16%), and generally occurs as bundles with an average OD of 1.97 ± 0.40 nm (Fig. 1A). CNTs-2 are mainly DWNTs (65%) with OD = 3.3 ± 0.89 nm

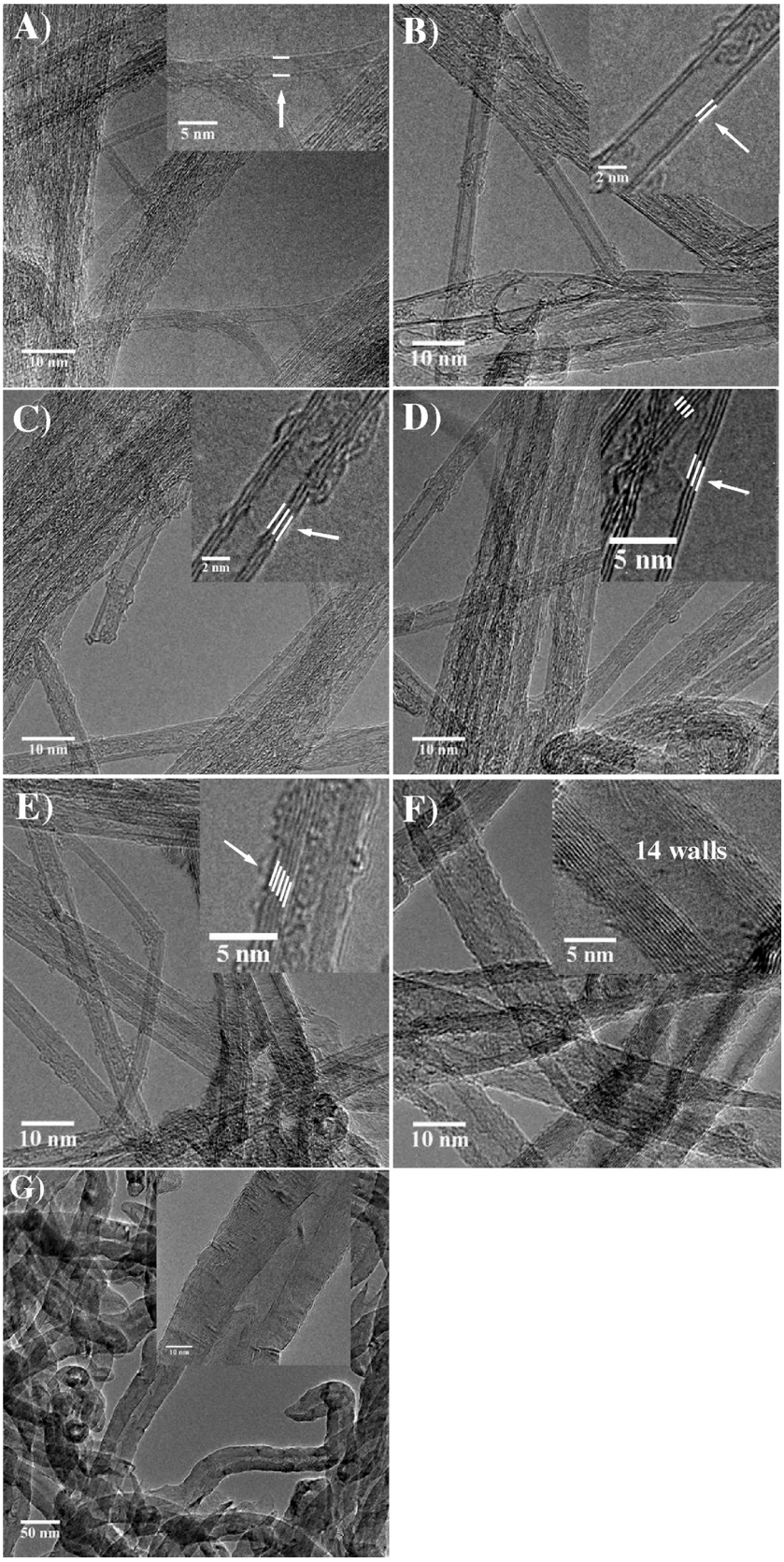

Fig. 1. TEM micrographs of CNTs samples. (A) CNTs-1, mainly SWNTs (79%) with OD = 1.97 nm, (B) CNTs-2, mainly DWNTs (65%) with OD = 3.3 nm, (C) CNTs-3, mainly TWNTs (52%) with OD = 3.8 nm, (D) CNTs-4, mainly TWNTs (57%) with OD = 4 nm, (E) CNTs-5, mainly CNTs with 3–10 walls and OD = 5.1 nm, (F) CNTs-6, mainly MWNTs with more than 12 walls and OD = 13.9 nm, and (G) CNTs-7, typical MWNTs with the number of walls exceeding 30 and OD = 20–40 nm.

Table 1
BET surface area, outer diameter, number of walls, I_D/I_G ratios of CNTs used in the present study.

CNTs	CNTs-1	CNTs-2	CNTs-3	CNTs-4	CNTs-5	CNTs-6	CNTs-7
Number of walls	1 (79%) 2 (16%) 3 (5%)	2 (65%) 3 (23%) 4 (5%)	2 (25%) 3 (52%) 4 (10%) 5 (8%)	3 (57%) 4 (20%) 5 (19%)	3 (5%) 4 (11%) 5 (25%) 6 (17%) 7 (16%) 8 (17%) 9 (9%)	>12	>30
n[a]	1	2	3	3	7	>12	>30
Outer diameters (nm)	1.97 ± 0.4	3.3 ± 0.89	3.8 ± 0.63	4.0 ± 0.66	5.1 ± 0.98	13.9 ± 5.2	35.2 ± 8.5
Surface area ($m^2\ g^{-1}$)	651	679	643	459	485	174	85
I_D/I_G	0.16	0.51	0.76	0.94	1.35	2.50	2.86

[a] n is the average of number of walls of CNTs samples, taking as an integer number.

(Fig. 1B), while CNTs-4 is similar to CNTs-3 mainly with triple-walled CNTs (TWNTs, 52–57%) and OD = 3.8–4 nm (Fig. 1C and D). As the number of walls increases to 3–10 (the average number of walls is taken as 7), the OD also increases to 5.1 ± 0.98 nm for CNTs-5 (Fig. 1E). CNTs-6 and CNTs-7 are MWNTs with the number of walls exceeding 12 and OD = 15–35 nm (Fig. 1F and G). The BET surface areas vary from 643 to 679 $m^2\ g^{-1}$ for CNTs-1, 2 and 3 to 175–85 $m^2\ g^{-1}$ for MWNTs. The number of walls, OD and BET surface areas of CNTs used in this study are given in Table 1.

Raman spectra provide more details on the CNTs with different sizes and number of walls (Fig. 2). For CNTs-1, the radial breathing mode (RBM) observed around CNTs 200–300 cm^{-1} is typical characteristics for SWNTs [24–26]. For CNTs-2 and CNTs-3, the intensity of RMB is much smaller and no RMB was observed for large diameter CNTs-4, CNTs-5, CNTs-6 and CNTs-7. The Raman spectra show that the intensities of the G band (~1590 cm^{-1}) and G' band (~2700 cm^{-1}) decrease with an increasing number of walls and OD. The ratio of the intensity of the D band near 1300 cm^{-1} to the G band, I_D/I_G is 0.155, 0.51, 0.76, 0.94, 1.35, 2.50 and 2.86 for CNTs-1; CNTs-2, CNTs-3, CNTs-4, CNTs-5, CNTs-6 and CNTs-7, respectively. The I_D/I_G ratio increases with the increasing number of walls and OD as multiple graphite layers lead to a greater quantity of structural defects [24,25]. The dominant RBM peaks and much smaller I_D/I_G observed on CNT-1 indicate that CNTs-1 is dominated by SWNTs,

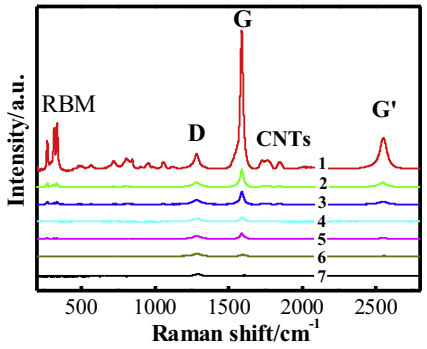

Fig. 2. Raman spectra of CNTs with different OD and number of walls.

while for CNTs-2 and CNTs-3, the dominant CNTs are DWNTs and TWNTs, respectively. These results are consistent with that of the high-resolution TEM images as shown in Fig. 1.

Fig. 3 is the TGA curves of CNTs samples before and after the HCl purification treatments. The as-received CNTs-1, CNTs-6 and CNTs-7 contain ~2 wt% ash, and it is ~5 wt% for CNTs-2, CNTs-3, CNTs-4 and CNTs-5. The composition of metal elements in CNTs before and after purification was analyzed by ICP, and the results are present

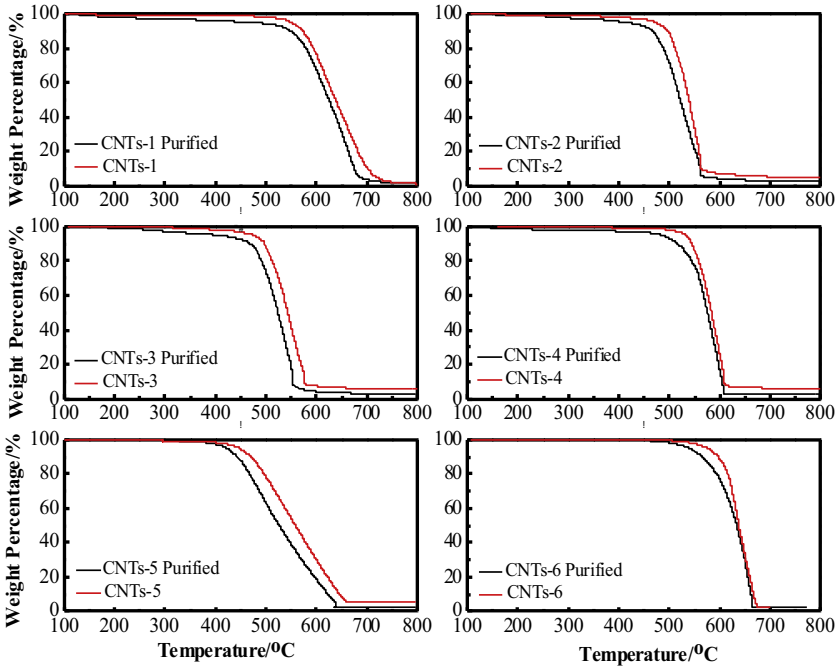

Fig. 3. TGA curves of CNTs before and after purification treatment.

Table 2
Metal impurity composition in as-received and purified CNTs by ICP.

CNTs		CNTs-1	CNTs-2	CNTs-3	CNTs-4	CNTs-5	CNTs-6	CNTs-7
As-received (w/w%)	Ash	1.56	4.82	5.1	5.2	5.16	2.16	2.39
	Co	0.08	2.32	2.02	–	0.5	–	–
	Fe	0.43	0.30	0.26	0.29	0.35	0.28	0.54
	Mo	0.04	0.75	0.73	0.79	0.11	–	0.84
	Ni	0.08	0.08	0.04	0.17	0.019	0.25	0.21
Purified (w/w%)	Ash	1.21	2.08	2.15	2.54	2.28	2.08	1.83
	Co	0.07	0.81	0.57	–	0.38	–	–
	Fe	0.29	0.23	0.23	0.28	0.17	0.21	0.29
	Mo	0.03	0.30	0.27	0.34	0.09	0.01	0.49
	Ni	0.05	0.04	0.03	0.15	0.015	0.2	0.17

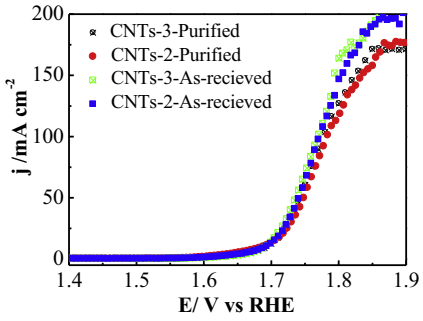

Fig. 4. Liner scans voltammetry of as-received and purified CNTs-2 and CNTs-3 for OER. The curves were measured at scan rate of 1 mV s^{-1} in 1 M KOH solution with CNTs loading of 0.025 mg cm^{-2}.

in Table 2. The trace metal elements in ash contain Fe, Co, Ni and Mo. The results indicate that the total amount of trace metals was reduced considerably after purification. For example, as-received CNTs-2 and CNTs-3 contain about 2.32 wt% and 2.02 wt% Co, and after purification, only 0.81 wt% and 0.57 wt% Co were detected in CNTs-2 and CNTs-3, respectively. The amount of Mo is also reduced by more than 50% after purification.

Fig. 4 is the electrochemical activity for OER on CNTs-2 and CNTs-3 before and after the purification treatment. The activity of CNTs after purification is slightly lower than that of as-received CNTs, despite the significant reduction in the trace elements in the as-received CNTs samples. For example, the as-received CNTs-2 contains 3.45 wt% trace metals such as Co, Fe, Mo, and Ni. After HCl purification, the trace metal contents are reduced to 1.38 wt%, 2.5 times lower than that in the received sample. Similar reduction in the trace metal elements was also observed for CNTs-3. However, the electrochemical activity of CNTs-2 and CNTs-3 for OER before and after purification treatment is very close, indicating that the presence of trace metals on the electrocatalystic activity of CNTs for OER is minor and can be ignored under the conditions of the present study.

3.2. Electrochemical activity for OER

Fig. 5A shows the typical linear scan voltammetry (LSV) curves of CNTs for the OER measured in 1 M KOH solution at rotating rate of 2000 rpm with a scan rate of 1 mV s^{-1}. Fig. 5B and C are the plots of the average current densities measured at 1.8 V (vs RHE) and the onset potential of the OER on CNTs against the tube size or the number of walls. The CNTs loading was 0.025 mg cm^{-2}. The electrocatalystic activity of CNTs for OER strongly depends on the characteristics of CNTs (i.e., OD and the number of walls). CNTs-2, CNTs-3 and CNTs-4 show significantly higher activity for the OER than those with CNTs-1, CNTs-5, CNTs-6 and CNTs-7. For the reaction on the CNTs-1, the onset potential is 1.75 ± 0.01 V and the current is 5.9 ± 1.7 mA cm^{-2} measured at 1.8 V. When the average number of walls increased to 3 with a corresponding increase of the tube size to OD = 3.8 nm (i.e., CNTs-3), the onset potential was shifted to a lower potential, 1.64 ± 0.01 V and the current density significantly increased to 56 ± 4.7 mA cm^{-2} at 1.8 V, almost 10 times higher than that measured on SWNTs, CNTs-1. However, with a further increase in the number of walls (or the tube size), the activity for OER decreases again. For example, for CNTs-5 with an average 7 walls and OD = 5.1 nm, the onset potential increased again to 1.73 ± 0.02 V and current density at 1.8 V dropped significantly to 28.7 ± 2.7 mA cm^{-2}. In the case of large diameter MWNTs (CNTs-7), the onset potential is around 1.78 ± 0.01 V and current density at 1.8 V is only 1.6 ± 1.8 mA cm^{-2}. Most significantly, the activity of CNTs for OER follows distinctive volcano-type dependence on the size (Fig. 5B) or on the number of walls of CNTs (Fig. 5C). The most active CNTs for the OER in alkaline solutions are the ones mainly with 2–7 walls and a diameter in the range of 2–5 nm (Fig. 5B and C).

The turnover frequencies (TOF) of CNTs and 50% Pt/C catalysts for the OER were calculated based on that reported by Yeo and Bell [27] (for detailed calculation, see Supporting information) and the results are given in Fig. 5D for the TOF values for the current densities measured at 1.8 V (vs RHE). The results show that the TOF increase from 0.01 s^{-1} for CNTs-1 to 1.34 s^{-1} for CNTs-2 and reach the maximum of 2.0 s^{-1} for CNTs-4, which is about twice of 0.954 s^{-1} measured on 50% Pt/C. As the number of walls increases, the TOF decreases again, 1.6 s^{-1} for the OER on CNTs-5 and 0.67 s^{-1} on CNTs-6 when the number of walls exceeds 12. Similar distinctive volcano-type dependence of TOF on the number of walls further demonstrates that the most active CNTs for the OER in alkaline solution are the ones with 2–7 walls and an outer diameter in the range of 2–5 nm.

For the purpose of comparison, the activities of activated carbon, graphite, 20% Ru/C and 50% Pt/C catalysts were measured for OER in alkaline solution under identical conditions and the results are given in Fig. 6 together with the results on CNTs-3 and CNTs-4. CNTs-3 and CNTs-4 have a lower onset potential and significantly higher current density, as compared with 50% Pt/C, activated carbon and graphite. For example, the current density of 56 ± 4.7 mA cm^{-2} at a potential of 1.8 V for the OER on CNTs-3 is 10 times that of 50% Pt/C (5.6 ± 2.1 mA cm^{-2}) and activated carbon (5.8 ± 3.2 mA cm^{-2}), and almost 100 times that of graphite (0.6 ± 1.2 mA cm^{-2}). The BET surface area of activated carbon and graphite is 651 and 679 m^2 g^{-1}, respectively, similar to that of CNTs-3 (643 m^2 g^{-1}, Table 1). This indicates that the high electrocatalytic activity of CNTs-3 for OER is not due to the high surface area. The onset potential of CNTs-3 for OER is 1.64 ± 0.01 V, which is 10 mV lower than that for Pt/C. The state-of-the-art Ru/C catalysts exhibited lowest onset potential of 1.58 ± 0.02 V, but the current density at 1.8 V for OER is only 23 ± 3.4 mA cm^{-2}, significantly lower than 47–56 mA cm^{-2} measured on CNTs-2, CNTs-3 and CNTs-4 under identical test conditions.

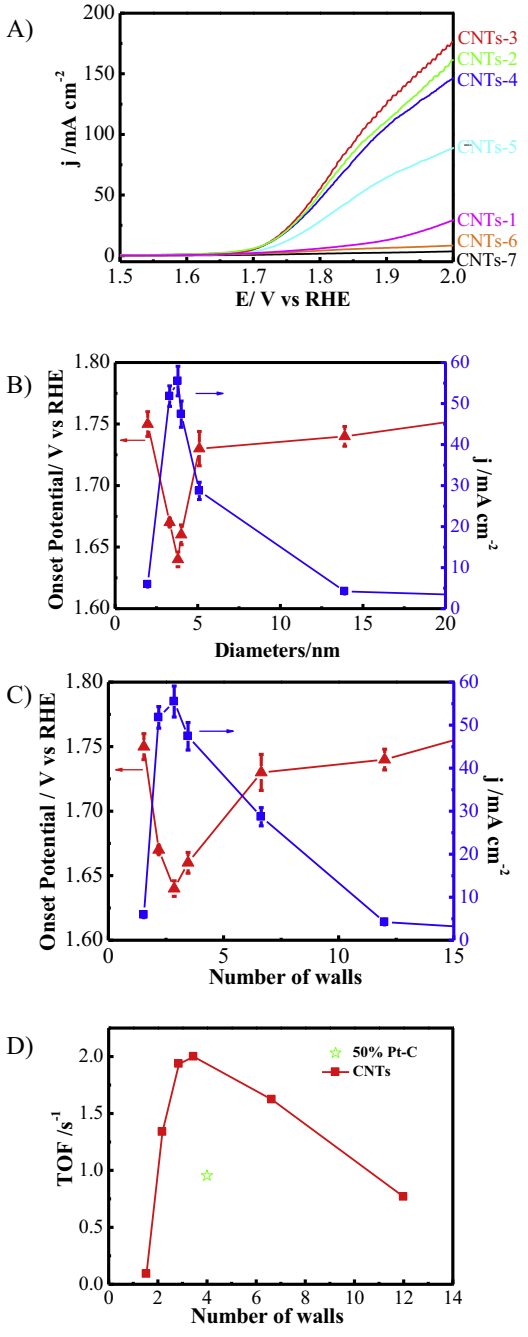

Fig. 5. (A) Linear scans voltammetry curves of OER for CNTs measured in 1 M KOH at scan rate of 1 mV s^{-1} with rotating rate of 2000 rpm; plots of current density measured at 1.8 V vs RHE and onset potential as a function of (B) outer diameter and (C) number of walls of CNTs; and (D) the calculated TOF vs the number of walls for CNTs and Pt/C catalysts at potential of 1.8 V vs RHE. The Pt/C catalyst and CNTs loading was 0.025 mg cm^{-2}.

The electrocatalytic activity of the CNTs for OER was further investigated by chronopotetiometry at different current densities with CNTs loading of 0.1 mg cm^{-2}, measured at a rotating rate of 2000 rpm. The results are shown in Fig. 7A. The potential for CNTs-2, CNTs-3, CNTs-4, CNTs-5 to deliver a current density of 2, 5, 10, 20 and 50 mA cm^{-2} is significantly lower than that of CNTs-1, CNT-6 and CNTs-7. For example, the potentials for CNTs-3 to achieve a current density of 2, 5, 10, 20 and 50 mA cm^{-2} are 1.64, 1.65, 1.68, 1.7 and 1.76 V, respectively. On the other hand the potentials for MWNTs, CNTs-6 to achieve a current density of 2, 5, 10, 20 and 50 mA cm^{-2} are 1.74, 1.87, 1.95, 2.4 and 2.6 V,

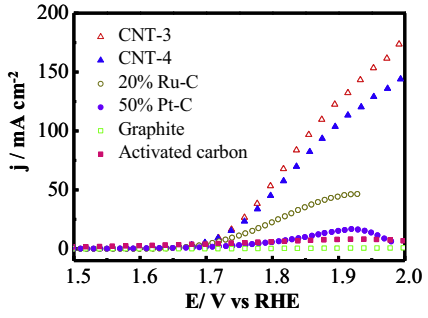

Fig. 6. Linear scans voltammetry curves of selected CNTs, activated carbon, graphite, 20% Ru/C and 50% Pt/C electrocatalysts for OER in 1 M KOH at a scan rate of 1 mV s^{-1} with rotating rate of 2000 rpm. The catalyst and CNTs loading was 0.025 mg cm^{-2}.

substantially higher than that observed on CNTs-3. These results further demonstrate that the electrocatalytic activity of CNTs-2, CNTs-3, CNTs-4 and CNTs-5 for OER is superior to CNTs-1, CNTs-6 and CNTs-7. The electrocatalytic activity of CNTs composed of between 2 and 7 concentric tubes and an OD of 2–5 nm is also comparable with the active transition metal oxides [28,29]. For example, the mass specific current density for OER on CNTs-3 is 100 A g^{-1} (i.e., 10 mA cm^{-2} on CNTs-3 with CNT loading of 0.1 mg cm^{-2}) at $\eta = 0.45$ V (1.68 V vs RHE), which is significantly better than 20 A g^{-1} reported on $NiMoO_4$ catalysts supported on Ni [29] and is comparable with 120 A g^{-1} for OER observed on the nitrogen-doped carbon materials under the same η [22]. Pristine CNTs are inherently very stable and highly conductive, an essential requirement as practical electrocatalysts for water oxidation reactions.

The stability of CNTs-3 was also measured and compared with the conventional 20% Ru/C, one of the best electrocatalysts for OER, at a current density of 10 mA cm^{-2} (Fig. 7B). The potential to achieve 10 mA cm^{-2} for CNTs-3 is 1.68 V ($\eta = 0.45$ V), 0.04 V higher than 20% Ru/C. McCrory et al. [28] recently studied the OER in

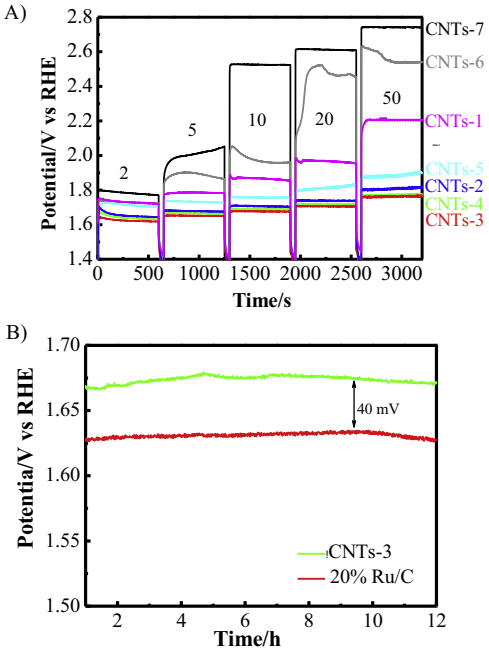

Fig. 7. (A) Chronopotentiometry curves of CNTs in 1 M KOH solution measured at different current densities and (B) stability plots of CNTs-3 and 20% Ru/C electrocatalysts measured in 1 M KOH at 10 mA cm^{-2}. The CNTs and Ru/C catalyst loading was 0.1 mg cm^{-2} and the rotating rate was 2000 rpm. Numbers in (A) are the current densities in mA cm^{-2}.

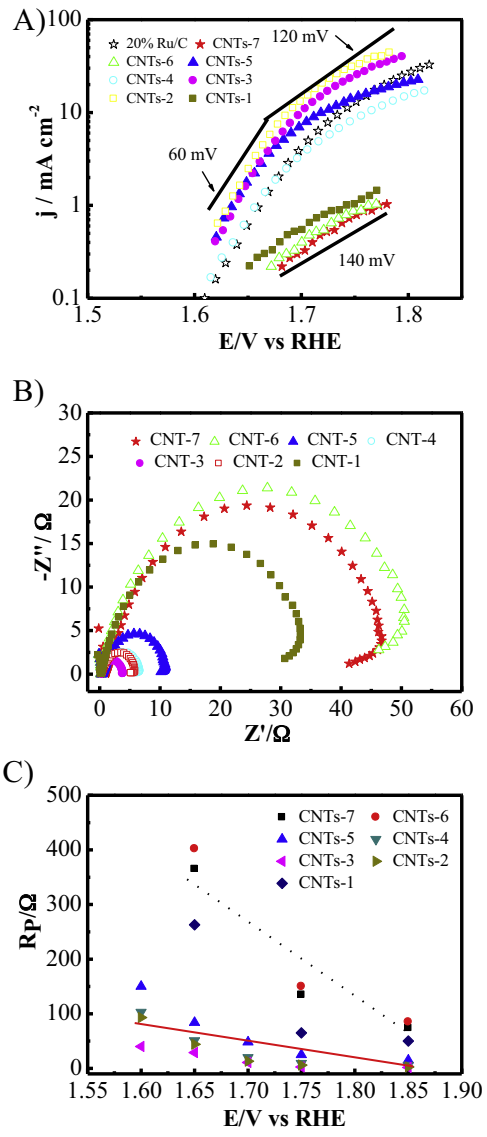

Fig. 8. (A) Tafel plots for the OER on CNTs and 20% Ru/C electrocatalysts, (B) impedance spectra for the OER on CNTs, measured at 1.65 V, and (C) electrode polarization resistance, R_P of CNTs as a function of the applied potential. The tests were conducted in 1 M KOH solution with catalyst loading of 0.025 mg cm^{-2}.

1 M KOH on the state-of-the-art heterogenous electrocatalysts prepared by electrodeposition. The η for achieving a current density of 10 mA cm^{-2} for IrO_x, $NiFeO_x$, $CoFeO_x$, $NiCoO_x$, CoO_x, $NiLaO_x$, $NiCuO_x$, NiO_x, and $NiCeO_x$ catalyst films varied from 0.32 to 0.43 V. Liang et al. [30] showed that Co_3O_4 nanocrystals grown on reduced graphene oxide (Co_3O_4/N-rmGO) exhibits a current density of 10 mA cm^{-2} at η = ~0.31 V in 1 M KOH solution with catalyst loading of 1 mg cm^{-2}. In the case of CNTs-3, the η to achieve 10 mA cm^{-2} is 0.45 V, 10–140 mV higher than the state-of-the-art Ru/C and heterogeneous electrocatalysts for OER. However, as shown in Fig. 6, pristine CNTs-3 has a substantial high current output at high overpotentials as compared to Ru/C and Pt/C electrocatalysts. The very stable performance of CNTs-3 as a function of polarization time also demonstrates that the pristine CNTs are stable and practical electrocatalysts for water oxidation reactions.

3.3. Kinetics of OER on CNTs

Fig. 8A is the Tafel plots for the OER on CNTs measured in 1 M KOH with catalysts loading of 0.025 mg cm^{-2}. Dual Tafel slopes were exhibited for the OER on CNTs-2, CNTs-3, CNTs-4 and CNTs-5, with a Tafel slope close to ~60 mV dec^{-1} at low η and ~120 mV dec^{-1} at high η. The dual Tafel slopes at low and high η regions were also reported for the OER on Pt and cobalt electrodes in alkaline solutions [3,31,32]. For the reaction on Ru/C, Tafel slope was 50 mV dec^{-1} at low η, similar to the Tafel slopes observed on metal oxide catalysts such as NiO_x and $(Ni,Co)O_x$ [33,34]. On the other hand, for the OER on CNTs-1, CNTs-6 and CNTs-7, the observed Tafel slope is ~140 mV dec^{-1}, substantially higher than that for the reaction on CNTs-2, CNTs-3, CNTs-4, CNTs-5 and Ru/C. The low Tafel slope values of ~60 mV dec^{-1} observed for the OER on CNTs-2, CNTs-3, CNTs-4, and CNTs-5 indicate the facile initial discharge of an OH^- ion on the surface of the outer walls of CNTs, as predicted for the first electron transfer step at the metal or metal hydroxide active site in the alkaline solution on metal and metal oxide-based catalysts [31,34,35]. The very high Tafel slope, ~140 mV dec^{-1} observed for the reaction on CNTs-1, CNTs-6 and CNTs-7 simply implies that the energy barrier for the electron transfer associated with the discharge of OH^{-1} species on the SWNTs and MWNTs is very high. This is evidently supported by the extremely low activity of SWNTs and MWNTs for the OER in alkaline solutions.

The electrochemical impedance responses for the OER on CNTs are characterized by a single and depressed arc (Fig. 8B), similar to that reported for the reaction on nickel and cobalt electrode [31,34]. The electrode polarization resistance, R_P is related to the kinetics of the interfacial charge transfer process. R_P for OER measured at a dc bias of 1.65 V (η = 0.42 V) on CNTs composed of between 2 and 7 concentric tubes and an outer diameter of 2–5 nm is in the range of 3.6–6.1 Ω cm^2, substantially smaller than 33 Ω cm^2 to 55 Ω cm^2 measured on CNTs-1, CNTs-6 and CNTs-7. And the R_P of CNTs composed of between 2 and 7 concentric tubes and an outer diameter of 2–5 nm are much less sensitive to the applied dc bias, indicating the high activity of the CNTs for the OER (Fig. 8C). These results again indicate the much lower energy barrier for OER on CNTs-2, CNTs-3, CNTs-4 and CNTs-5, as compared to the reaction on CNTs-1, CNTs-6 and CNTs-7, consistent with the results from LSV and Tafel slope.

3.4. Electrocatalytic activity of CNTs

Wang et al. [36] showed recently that the trace metal elements in the heteroatom-doped graphene are responsible for the observed catalytic oxygen reduction reaction. In the present study, the amount of trace metal impurities (i.e., Co, Fe, Mo, Ni) in the as-received CNTs samples are typically in the range of 0.63% for CNTs-1 to 3.45% for CNTs-3 (see Table 2). After HCl treatment, the total trace metal impurities are reduced to 1.3% for CNTs-2, 1.1% for CNTs-3, and 0.44% for CNTs-1. The presence of the trace metal impurities after the HCl treatment is mainly due to the fact that milder purification treatment was used in this study to avoid the adverse structural modification of CNTs associated with harsh oxidation treatment [37]. As shown in Fig. 3, significant reduction in the trace metal impurities has little effect on the electrocatalytic activity of the selected CNTs for the OER in alkaline solutions. The activity of CNTs-3 for OER is almost 10 times higher than that measured on CNTs-1 while the content of trace metal impurities of CNTs-3 is 1.1%, about 2.5 times higher than 0.44% on CNTs-1. The activity of MWNTs, CNTs-7, is 35 times lower than that of CNTs-3, but the trace metal content of CNTs-7 is 0.95%, close to that of CNTs-3 (Table 2). These results indicate that the presence of trace metal impurities is not responsible for the remarkable difference of the activities between CNTs samples.

Having identified that there is a clear maximum in the catalytic activity of CNTs as a function of increasing size or number of walls, it is important to consider whether there is a rationale for this observed behavior. As a starting point, the energetics of functionalization of CNTs as a function of diameter has been extensively

examined for a variety of substituents. For example, it is well documented that processes such as the chemisorption of hydrogen on the outside surface of SWNTs is exothermic for small diameters, due to the release of strain, and becomes less favorable as the index, *n*, of the armchair nanotube (n, n) increases [38,39]. Based on these, and similar results for other chemical reactions at the CNT outer surface, it might be expected that the initial reaction of hydroxide, i.e., the discharge of OH^{-1} species and other mechanistic steps that involve adsorption or attachment of OH^{-1} species to the outer walls of the tubes, are most favorable and therefore fastest for CNTs of smallest diameter. Therefore it might be expected that the rate would diminish with increasing CNT size. While this is in accord with the limiting behavior observed for larger diameters, it fails to explain why CNTs with outer diameter 2–5 nm are far more effective than the single walled CNTs with smaller size.

The electron transport properties of CNTs can play an important role in the charge transfer processes for the OER. The electric properties of SWNTs are sensitive to the size and chirality of the tubes. In theory, nearly one-third of the SWNTs are metallic or semi-metallic and the other two-thirds are semiconducting [40]. The absorption of OH^- and intermediate species, such as OOH^*, could have a significant effect on the electronic state of the outer wall of SWNTs as it is well known that covalent sidewall functionalization of SWNTs can drastically change the electronic states of nanotubes near the Fermi level [41]. The covalent functionalization associated with the purification of CNTs could disrupt the π-electron system, causing the loss of the optical and electrical properties of SWNTs. The combined effect of dominant semiconducting properties and variation of electronic states by absorption of OH^- and other species could be responsible for the low activity of the SWNTs (i.e., CNTs-1) for OER and fuel cell reactions.

Unlike SWNTs, the presence of inner walls could increase the number of conducting channels and create the possibility of interactions between the different walls. Fujisawa et al. [42] studied the electrical properties of SWNTs and DWNTs and showed experimentally that the conduction mechanism strongly depends on the total fraction of metallic inner and outer tubes within the DWNT samples, and the inner tubes contribute significantly to the electronic transport properties of DWNTs. The outer wall can also serve as a protective barrier to prevent endohedral reactions, potentially allowing the inner tube to retain its electronic properties [43]. This indicates the possibility of the separation of functionality of the outer wall and inner tubes for the OER on DWNTs; the outer wall provides reaction sites for the adsorption and dissociation of OH^-, OOH^*, species, while the intact inner tube serves as the electronic conducting pathway for the charge transfer process of the reaction, assuming there is a reasonable distribution of conducting and semiconducting tubes for both outer wall and inner tubes. The electron transfer between the outer wall and inner tube could occur by electron tunneling, similar to the electron tunneling through thin oxide films as proposed by Damjanovic et al. [44] for the OER on Pt. This hypothesis explains why double/triple-walled CNTs-2, CNTs-3 and CNTs-4 are far more effective than single-walled CNTs-1.

As the number of walls/layers increases, other issues could adversely affect the electrocatalytic activity of CNTs. Li et al. [45] studied the transparency-conductance performance of SWNTs, DWNTs and MWNTs, and found that DWNTs have better performance in this regard. This was explained by the fact that SWNTs contain many semi-conducting nanotubes, while MWNTs materials absorb more photons per nanotube due to the large mass density. In the case of OER, the driving force for the electron transfer or tunneling between the outer wall and inner tubes is the applied dc bias, i.e., the η. As the number of walls/layers increases, the dc bias between the outer wall and the nearest inner tube would diminish due to the distribution of the dc bias, i.e., the driving force, across each layer. Thus, the electron transfer or tunneling from the outer surface to the inner tubes could become less favorable as the number of walls/layers increases. This appears to be supported by the reduced activity of CNTs-5 as compared to CNTs-2, CNTs-3 and CNTs-4 due to the increased number of walls, and the very high Tafel slope and high R_P for the OER on multi-walled CNTs-6 and CNTs-7. The volcano-type dependence of the activity of CNTs for the OER in alkaline solutions as a function of number of walls of CNTs is schematically shown in Fig. 9.

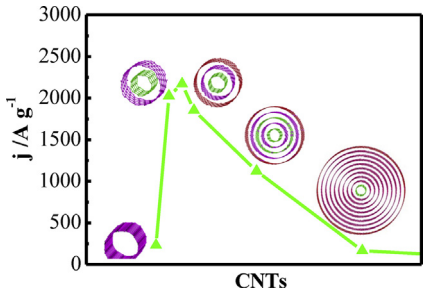

Fig. 9. Plot of the activity of CNTs for the OER in 1 M KOH solutions as a function of number of walls. The mass specific activity was measured at 1.8 V (vs RHE) at scan rate of 1 mV s^{-1} and rotating rate of 2000 rpm with CNTs loading of 0.025 mg cm^{-2}.

4. Conclusion

Here we demonstrated, for the first time, that the electrocatalytic activity of CNTs for the OER of water electrolysis in alkaline solutions shows a distinctive volcano-dependence on the size and/or the number of walls of CNTs. CNTs with OD around 2–5 nm and 2–7 walls have excellent activity, fast kinetics and much lower energy barrier for OER in alkaline solutions, as compared with the SWNTs (i.e., CNTs-1) and MWNTs (i.e., CNTs-6 and CNTs-7). For example, the activity of TWNTs (i.e., CNTs-3) measured at 1.8 V (vs RHE) for OER is ~10 times higher than that observed on SWNTs and 35 times higher than that on MWNTs. The Tafel slope for the reaction on CNTs with OD around 2–5 nm and 2–7 walls is ~60 mV dec^{-1}, substantially lower than ~140 mV dec^{-1} for the reaction on SWNTs and MWNTs, i.e., CNTs-1, CNTs-6 and CNTs-7. Such CNTs are also very active as compared to conventional 50% Pt/C and 20% Ru/C electrocatalysts in alkaline solutions. Substantial work needs to be done to fundamentally understand the reasons for the volcano-type dependence of the activity of CNTs for the OER in alkaline solutions. Preliminary results indicate that there may exist a dual functionality of CNTs with specific number of walls; the outer wall provides reaction sites for the absorption and dissociation of OH^-, OOH^*, species, while the intact inner-tube serves as the effective electronic conducting pathway for the charge transfer process of the reaction via electron tunneling between the outer wall and inner tubes. However, such dual functionality of the CNTs for OER diminishes as the number of walls increases most likely due to the reduced driving force (i.e., the dc bias) across the walls or layers of CNTs for the electron tunneling between the outer wall and inner tubes.

Acknowledgments

This research was supported by the Australian Research Council *Discovery Project Funding Scheme* (project number: DP120102325, DP120104932 and DP0986999), and the Major International (Regional) Joint Research Project of the National Natural Science Foundation of China (51210002), as well as the access to resources at iVEC and NCI.

Appendix A. Supplementary data

Supplementary data associated with this article can be found, in the online version, at http://dx.doi.org/10.1016/j.apcatb.2014.07.049.

References

[1] J.R. McKone, N.S. Lewis, H.B. Gray, Chem. Mater. 26 (2014) 407–414.
[2] T.J. Meyer, Nature 451 (2008) 778–779.
[3] V.I. Birss, A. Damjanovic, J. Electrochem. Soc. 134 (1987) 113–117.
[4] T. Reier, M. Oezaslan, P. Strasser, ACS Catal. 2 (2012) 1765–1772.
[5] D.V. Esposito, S.T. Hunt, Y.C. Kimmel, J.G. Chen, J. Am. Chem. Soc. 134 (2012) 3025–3033.
[6] J.C. Cruz, V. Baglio, S. Siracusano, V. Antonucci, A.S. Arico, R. Ornelas, L. Ortiz-Frade, G. Osorio-Monreal, S.M. Duron-Torres, L.G. Arriaga, Int. J. Electrochem. Sci. 6 (2011) 6607–6619.
[7] E. Rasten, G. Hagen, R. Tunold, Electrochim. Acta 48 (2003) 3945–3952.
[8] A. Di Blasi, C. D'Urso, V. Baglio, V. Antonucci, A.S. Arico, R. Ornelas, F. Matteucci, G. Orozco, D. Beltran, Y. Meas, L.G. Arriaga, J. Appl. Electrochem. 39 (2009) 191–196.
[9] T. Takashima, K. Hashimoto, R. Nakamura, J. Am. Chem. Soc. 134 (2012) 1519–1527.
[10] W.Y. Yuan, P.K. Shen, S.P. Jiang, J. Mater. Chem. A 2 (2014) 123–129.
[11] R.N. Singh, D. Mishra, Anindita, A.S.K. Sinha, A. Singh, Electrochem. Commun. 9 (2007) 1369–1373.
[12] J. Wu, Y. Xue, X. Yan, W. Yan, Q. Cheng, Y. Xie, Nano Res. 5 (2012) 521–530.
[13] C.R. Davidson, G. Kissel, S. Srinivasan, J. Electroanal. Chem. 132 (1982) 129–135.
[14] M.W. Louie, A.T. Bell, J. Am. Chem. Soc. 135 (2013) 12329–12337.
[15] R.D.L. Smith, M.S. Prévot, R.D. Fagan, S. Trudel, C.P. Berlinguette, J. Am. Chem. Soc. 135 (2013) 11580–11586.
[16] D. Eder, Chem. Rev. 110 (2010) 1348–1385.
[17] F.M. Toma, A. Sartorel, M. Iurlo, M. Carraro, S. Rapino, L. Hoober-Burkhardt, T. Da Ros, M. Marcaccio, G. Scorrano, F. Paolucci, M. Bonchio, M. Prato, ChemSusChem 4 (2011) 1447–1451.
[18] M. Gong, Y. Li, H. Wang, Y. Liang, J.Z. Wu, J. Zhou, J. Wang, T. Regier, F. Wei, H. Dai, J. Am. Chem. Soc. 135 (2013) 8452–8455.
[19] Y. Xiang, S. Lu, S.P. Jiang, Chem. Soc. Rev. 41 (2012) 7291–7321.
[20] X. Lu, C. Zhao, J. Mater. Chem. A 1 (2013) 12053–12059.
[21] F. Li, B. Zhang, X. Li, Y. Jiang, L. Chen, Y. Li, L. Sun, Angew. Chem. Int. Ed. 50 (2011) 12276–12279.
[22] Y. Zhao, R. Nakamura, K. Kamiya, S. Nakanishi, K. Hashimoto, Nat. Commun. 4 (2013).
[23] K.P. Gong, F. Du, Z.H. Xia, M. Durstock, L.M. Dai, Science 323 (2009) 760–764.
[24] U.J. Kim, C.A. Furtado, X.M. Liu, G.G. Chen, P.C. Eklund, J. Am. Chem. Soc. 127 (2005) 15437–15445.
[25] M.S. Dresselhaus, G. Dresselhaus, R. Saito, A. Jorio, in: S. Saito, A. Zettl (Eds.), Carbon Nanotubes: Quantum Cylinders of Graphene, Elsevier Science B.V., Amsterdam, 2008, pp. 83–108.
[26] R. Saito, M. Hofmann, G. Dresselhaus, A. Jorio, M.S. Dresselhaus, Adv. Phys. 60 (2011) 413–550.
[27] B.S. Yeo, A.T. Bell, J. Am. Chem. Soc. 133 (2011) 5587–5593.
[28] C.C.L. McCrory, S. Jung, J.C. Peters, T.F. Jaramillo, J. Am. Chem. Soc. 135 (2013) 16977–16987.
[29] R.N. Singh, M.R. Awasthi, A.S.K. Sinha, J. Solid State Electrochem. 13 (2009) 1613–1619.
[30] Y. Liang, Y. Li, H. Wang, J. Zhou, J. Wang, T. Regier, H. Dai, Nat. Mater. 10 (2011) 780–786.
[31] M.E.G. Lyons, M.P. Brandon, Int. J. Electrochem. Sci. 3 (2008) 1425–1462.
[32] A. Damjanovic, Electrochim. Acta 37 (1992) 2533–2539.
[33] L. Trotochaud, J.K. Ranney, K.N. Williams, S.W. Boettcher, J. Am. Chem. Soc. 134 (2012) 17253–17261.
[34] M.E.G. Lyons, M.P. Brandon, Int. J. Electrochem. Sci. 3 (2008) 1386–1424.
[35] R.L. Doyle, I.J. Godwin, M.P. Brandon, M.E.G. Lyons, Phys. Chem. Chem. Phys. 15 (2013) 13737–13783.
[36] L. Wang, A. Ambrosi, M. Pumera, Angew. Chem. Int. Ed. 52 (2013) 13818–13821.
[37] Z.Q. Tian, S.P. Jiang, Y.M. Liang, P.K. Shen, J. Phys. Chem. B 110 (2006) 5343–5350.
[38] H. Cheng, G.P. Pez, A.C. Cooper, J. Am. Chem. Soc. 123 (2001) 5845–5846.
[39] A. Bilic, J.D. Gale, J. Phys. Chem. C 112 (2008) 12568–12575.
[40] R. Saito, M. Fujita, G. Dresselhaus, M.S. Dresselhaus, Appl. Phys. Lett. 60 (1992) 2204–2206.
[41] J.J. Zhao, H.K. Park, J. Han, J.P. Lu, J. Phys. Chem. B 108 (2004) 4227–4230.
[42] K. Fujisawa, K. Komiyama, H. Muramatsu, D. Shimamoto, T. Tojo, Y.A. Kim, T. Hayashi, M. Endo, K. Oshida, M. Terrones, M.S. Dresselhaus, ACS Nano 5 (2011) 7547–7554.
[43] C. Shen, A.H. Brozena, Y.H. Wang, Nanoscale 3 (2011) 503–518.
[44] A. Damjanovic, V.I. Birss, D.S. Boudreaux, J. Electrochem. Soc. 138 (1991) 2549–2555.
[45] Z.R. Li, H.R. Kandel, E. Dervishi, V. Saini, A.S. Biris, A.R. Biris, D. Lupu, Appl. Phys. Lett. 91 (2007).